View metadata, citation and similar papers at core.ac.uk

brought to you by CORE

provided by NASA Technical Reports Server

NASA Technical Memorandum 105999

Laser Rayleigh and Raman Diagnostics for Small Hydrogen/Oxygen Rockets

Wilhelmus A. de Groot
Sverdrup Technology, Inc.
Lewis Research Center Group
Brook Park, Ohio

and

Frank J. Zupanc
National Aeronautics and Space Administration
Lewis Research Center
Cleveland, Ohio

Prepared for the
SPIE International Symposium on Lasers, Sensors, and Applications
sponsored by the Society of Photo-Optical Instrumentation Engineers
Los Angeles, January 16–23, 1993

(NASA-TM-105999) LASER RAYLEIGH AND RAMAN DIAGNOSTICS FOR SMALL HYDROGEN/OXYGEN ROCKETS (NASA) 17 p

N93-17995

Unclas

G3/20 0142864

Laser Rayleigh and Raman Diagnostics For Small Hydrogen/Oxygen Rockets

Wilhelmus A. deGroot
Sverdrup Technology, Inc.
Lewis Research Center Group
Brook Park, Ohio 44142

and

Frank J. Zupanc
National Aeronautics and Space Administration
Lewis Research Center
Cleveland, Ohio 44135

ABSTRACT

Localized velocity, temperature, and species concentration measurements in rocket flow fields are needed to evaluate predictive computational fluid dynamics (CFD) codes and identify causes of poor rocket performance. Velocity, temperature, and total number density information have been successfully extracted from spectrally resolved Rayleigh scattering in the plume of small hydrogen/oxygen rockets. Light from a narrow band laser is scattered from the moving molecules with a Doppler shifted frequency. Two components of the velocity can be extracted by observing the scattered light from two directions. Thermal broadening of the scattered light provides a measure of the temperature, while the integrated scattering intensity is proportional to the number density. Spontaneous Raman scattering has been used to measure temperature and species concentration in similar plumes. Light from a dye laser is scattered by molecules in the rocket plume. Raman spectra scattered from major species are resolved by observing the inelastically scattered light with a linear array mounted to a spectrometer. Temperature and oxygen concentrations have been extracted by fitting a model function to the measured Raman spectrum. Results of measurements on small rockets mounted inside a high altitude chamber using both diagnostic techniques are reported.

2. INTRODUCTION

Improving the performance of on-board rockets yields rewards in terms of extended mission life, or enhanced mission goals through a reduced propellant load.[1] Computational fluid dynamics (CFD) codes are routinely used both to evaluate rockets which are under development and to establish the effect of design changes on existing rockets. In some cases an acceptable prediction of rocket performance can be made with the current level of predictive technology. For high and medium thrust rockets, predictions of the global parameters such as thrust and specific impulse, show good agreement with measurements. Using these codes for predicting the performance of certain low thrust rockets, however, leads to inaccurate predictions, the specific causes of which are not identified.[2,3] Improved predictions for these rockets can only be made based on a better understanding of the physics of small rockets, a refined analysis of the individual rocket, and an increase in numerical capabilities. Such developments are aided by the availability of localized fluid dynamic and thermodynamic data upon which these improved codes can be verified.

The rockets tested in this investigation were gaseous hydrogen/oxygen rockets mounted inside a high altitude simulation chamber. The absence of ambient light inside the high altitude chamber combined with the low luminosity of the water vapor rich plume provided ideal conditions for spectroscopic probing by lasers. Laser Doppler anemometry requires the use of particles. The large gradients inherent in small rockets as well as the difficulties in introducing particles precluded the application of this technique to small rockets. This prompted the development of a technique based on Rayleigh scattering. This technique yields velocity and in some cases the temperature and number density of the molecules in a high velocity plume.[4] For Rayleigh scattering a narrow band laser beam (pulsed or cw) was directed through the plume. The laser light scattered from the moving molecules was Doppler shifted and collected at two locations. The magnitude of the observed Doppler shift is dependent on the relative angles between the incident and scattered light and the gas velocity. Since the relative angle between the incident and collection optics was known, the mean velocity of the observed gas volume was determined from the magnitude of the Doppler shifts measured at each location.

In addition to a mean gas velocity, each molecule possesses its own thermal motion which depends on the gas temperature and the molecular mass. When the gas is in thermal equilibrium, the molecular velocity obeys a Maxwellian distribution, which results in a Gaussian profile for the scattered laser light.[5] Therefore, in the absence of other significant broadening parameters, the degree of broadening for a single species can directly be related to the temperature. Accordingly, by resolving the line shape of the scattered light, and relating this to the reference laser line shape, it was possible to directly estimate the molecular velocity and translational temperature. Furthermore, since the scattering intensity for a single species is linearly proportional to the molecular number density, total number density could be estimated for the mixture by comparing the total scattered intensity and the intensity scattered by a reference gas.

Spontaneous Raman scattering was implemented for measuring temperature and species number densities. Light from a pulsed dye laser was focused in the rocket plume. Both Rayleigh and Raman scattering processes occur inside this focal volume. Raman scattering occurs when light photons exchange energy with rotational and/or vibrational internal molecular energy modes. Incident photons that lose energy to a molecular energy system are shifted to a lower spectral frequency. This spectral shift depends on the scattering species since these energy losses are discrete and equal to a change in molecular energy quantum. Thus each observed shifted spectral line indicates the presence of a specific species, characterized by the magnitude of the shift from the incident laser line. For a set of molecules in thermal equilibrium, the population over all possible energy levels can be described by a Boltzman distribution. Since quantum jumps are equally likely from all initial energy levels, the distribution of the Raman scattered photons over the different possible shifted lines for each species reflects this Boltzman distribution. Light scattered from the probe volume was collected and spectrally separated. Measurement of the intensity distribution of this light over the possible spectral range for the measured species yielded the Boltzman distribution from which the temperature was determined. The overall intensity of this distribution depends linearly on the incident laser intensity and on the number density of the scattering species. Because the laser intensity was known, the number density was directly determined from the scattered intensity.

Both techniques are impeded by the presence of ambient light. Raman scattering is a naturally weak process which requires minimum ambient and stray light to achieve acceptable signal to noise ratio (SNR). Rayleigh scattering is three orders of magnitude stronger and is therefore less sensitive to experimental conditions. However, for the measurements reported in this paper, the combined effects of low scattering number densities and the need for highly resolved spectra resulted in low signal levels. Judicious placement of pinholes, baffles and beam stops was therefore required to achieve an acceptable SNR. The limited number of windows of the high altitude simulation chamber were blocked to remove all ambient light, and extensive use was made of optical fibers for accessing the chamber.

Velocity and temperature measurements based on spectrally resolved Rayleigh scattering were successfully made on a lab model gaseous hydrogen/oxygen rocket engine with a nozzle area ratio of 30:1. The nozzle was modified for the Raman measurements since the number densities in the exit plane of the full scale rocket were prohibitively low. A reduced area ratio nozzle was installed which made number density and temperature measurements feasible in the exit plane. The results obtained with both techniques were compared to predictions by existing CFD codes. Results are reported in this paper.

3. ROCKET TEST FACILITY

The rockets tested were designed for space operation. To simulate a space environment, tests were conducted in a high altitude simulation chamber.[6] This chamber is 0.91 m in diameter and 1.81 m in length. The chamber is evacuated by means of a supersonic diffuser which is driven by a two stage venturi ejector stack. The 0.102 m diameter diffuser fully captured the rocket plume. The diffuser performance was optimized by locating the diffuser entrance from 0 to 0.10 m behind the rocket exit plane. When optical access was required, a trade-off between the diffuser distance and optical access was necessary. Under optimal conditions, chamber pressure was maintained at 1.3 kPa, simulating conditions at a height of 35 km. During tests when the plume was not captured sufficiently, the pressure gradually rose. Tests were usually aborted after the pressure exceeded 6.9 kPa. A detailed description of the high altitude simulation facility and the optical access is given in Ref. 6.

The rockets, shown schematically in Fig. 1 were in the 110 N thrust class.[2] They were designed to operate with gaseous hydrogen and oxygen with an oxygen-to-fuel ratio of 3.0-5.0. The propellant was supplied by high pressure trailers. A combination of upstream regulators and calibrated sonic venturis controlled the propellant flow rates to the thruster which

were continuously monitored. The 0.025 m diameter, 0.102 m long combustion chamber converged into a nozzle with a throat diameter of 0.0128 m and exit area ratio of 33:1. Gaseous hydrogen was used to regeneratively cool the combustion chamber and nozzle. The hydrogen entered wall passages through a channel in the nozzle exit plane and propagated upstream through the chamber walls toward the combustion chamber. The hydrogen flow was then split by means of calibrated flow passages. Part of the hydrogen was directed towards the core flow of the injector and part was diverted to a sleeve which distributed the fuel in a thin film over the combustion chamber wall. The amount of fuel diverted for fuel film cooling was regulated between 50% and 75%. The thruster injector was a stacked platelet injector. Oxygen was injected upstream of a spark plug and flowed past the spark plug tip towards the combustion chamber. At the spark plug tip, hydrogen was injected through radial passages in the stacked platelets into the oxygen flow and was entrained in the recirculation zone created behind the blunt spark plug tip. After initially igniting the oxygen rich mixture, the spark plug functioned as a flame holder, creating turbulent mixing and maintaining combustion. The oxygen rich product mixture entered the combustion chamber and gradually consumed the hydrogen fuel film at the wall.

Several conditions were favorable for applying Rayleigh scattering to the plume. The choice of propellants led to a plume with extremely low luminosity in the wavelength range of interest for Rayleigh scattering, providing an acceptable signal-to-noise ratio. Furthermore, the low pressure in the exit plane guaranteed that the mean-free-path between molecules was much larger than the scattering interaction wavelength. Accordingly it could be assumed that the scattering occurred in the "collisionless" regime, where uncorrelated scattering of molecules could be assumed. This greatly simplified the scattering analysis.[7]

The Rayleigh scattering analysis assumed water to be the single scattering species. Because the overall mixture ratio was fuel rich it is reasonable to assume that the plume was fuel rich. Water molecules have a much larger Rayleigh scattering cross section than hydrogen and the much lower molecular mass of hydrogen causes its scattering contribution to be spread over a much wider spectral range. Therefore water vapor was assumed to be the dominant scattering species. Due to the fuel film cooling however, there was a considerable variation in local mixture ratio, gradually varying from an oxygen rich core to a fuel rich perimeter region. As previously stated, water vapor was the dominant scatterer in those regions that were fuel rich. Oxygen contributed significantly to the total scattering for measurements in the core. This made it impossible to estimate the temperature and total number density.

The extremely low luminosity of the hydrogen-oxygen combustion products in the plume was also favorable for Raman scattering. As with the Rayleigh scattering, the low density made a simple, collision free analysis possible. However, the same low density made it difficult to detect Raman scattering in the exit plane during the 30 second test times. Therefore, for Raman scattering experiments, the nozzle length was reduced to an area ratio of 1.86:1. A simple one-dimensional nozzle analysis showed the pressure in this exit plane to be about 0.1 MPa., theoretically providing a sufficient number density for Raman scattering diagnostics. The redesigned test rocket wall was water cooled. The injected hydrogen which provided film cooling was lower in temperature than the hydrogen injected in the regeneratively cooled rocket. As a result, the fuel film injection velocity was different than during the Rayleigh experiments.

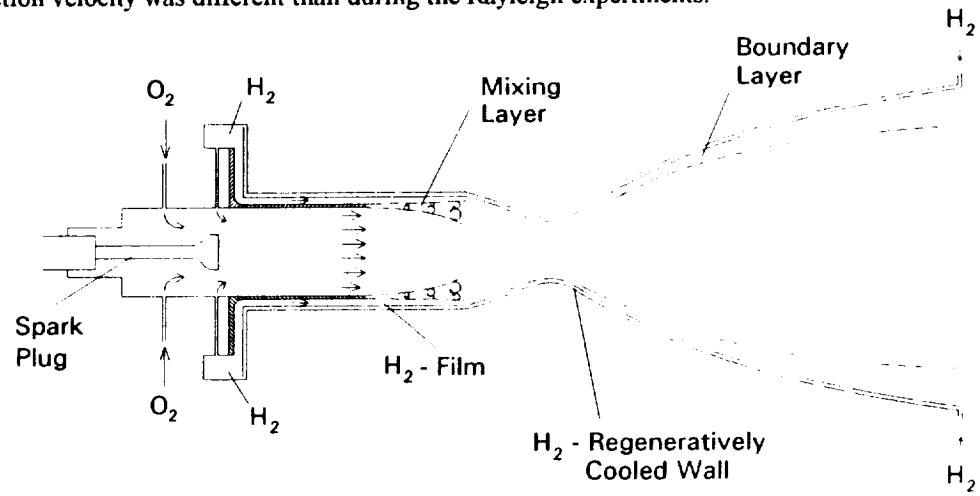

Fig. 1. Regeneratively cooled hydrogen-oxygen thruster flow field with fuel film cooling.

4. SPECTRALLY RESOLVED RAYLEIGH SCATTERING

Rayleigh scattering occurs when an incident electromagnetic wave and a molecule interact without exchanging energy. Three conditions have to be satisfied for a relatively simple treatment of both theory and application. The wavelength of the incident wave should be much larger than the size of the scattering molecule. If this is satisfied, a simple oscillating dipole is induced inside the molecule, which creates its own electromagnetic field and subsequent radiation (scattering). The dipole oscillates with the frequency of the incident wave, and consequently the scattered wave is of the same frequency. For a simple "collisionless" treatment of Rayleigh scattering theory, the scattering number densities have to be low enough to ensure that the collisional mean free path of the molecules is much larger then the interaction wavelength. If that is the case, the incident wave will interact with the molecules in an uncorrelated manner[7] and the resulting Rayleigh scattering is characterized by a simple Gaussian shape. Finally, the scattering volume should consist of a single component gas or the mixture composition should be known. When a wave is incident on a single component gas volume, the scattered intensity depends only on the molecular number density, and can be used for measuring number densities. Since the strength of the dipole that is created varies with type of molecule, the scattered intensity varies with type and number of scattering molecules. In addition, because the bandwidth of the Gaussian shape depends on the molecular weight, the contribution of each species to the final profile is a Gaussian of widely varying shape. It is therefore generally difficult to measure molecular number densities in a gas mixture if the gas composition is not known a priori.

The directionality of Rayleigh scattering depends on the polarization of the incident wave. For a linearly polarized incident wave, the dipole oscillates one-dimensionally and the radiation shows a toroidal distribution, with the strongest scattering perpendicular to the oscillating dipole. It is therefore important to detect the Rayleigh scattered radiation perpendicular to the electric field vector.

4.1 Theory

The random velocities of the individual molecules of a thermalized gas volume at rest follow a Maxwellian velocity distribution. Because of this, the Rayleigh spectrum that results when an incident plane wave of single frequency is scattered by this gas volume exhibits a Gaussian shape centered around the incident wavelength. This shape possesses a bandwidth (FWHM) which is directly proportional to the square root of the gas temperature. For a gas volume with mean velocity not equal to zero, the peak position of the observed spectrum is shifted from the incident wavelength. The shift depends on the gas velocity and the relative orientation between the incident and observed light, as illustrated in Fig. 2a for a backscatter and Fig. 2b for a forward scatter geometry. A detailed derivation shows that the power scattered by a single component gas in the direction of observation given by "scattered" vector $\bar{k}_s$ into solid angle $d\Omega$ in frequency interval df is:[4]

$$P_s(f)\, df\, d\Omega = I_0\, n\, V_{sc} \left[\frac{d\sigma}{d\Omega}\right] \sin^2\chi\ S(f)\ df\, d\Omega \qquad (1)$$

where I_0 is the incident irradiance in W/m^2, n the molecular number density in m^{-3}, and V_{sc} is the scattering volume. The differential Rayleigh scattering cross section $\left[\frac{d\sigma}{d\Omega}\right]$ is given in m^2/sr, and χ is the angle between the incident electric field vector $\bar{k}_0$ and $\bar{k}_s$. The frequency distribution function $S(f)$ is the normalized spectrum of Rayleigh scattered light. This normalized spectrum can be obtained by integrating the Maxwellian velocity distribution over the velocity space. This gives:[4]

$$S(f)\, df = \frac{2\sqrt{\pi}}{a\,K}\, e^{-(2\pi f - \bar{K}\cdot\bar{u})^2/a^2K^2}\, df \qquad (2)$$

where $a = (2\kappa T/m)^{1/2}$ is the "most probable speed" of the molecules in m/sec, and K is the scattering vector magnitude, where the scattering wave vector can be obtained from the relation $\bar{K} = \bar{k}_s - \bar{k}_0$. The thermodynamic constant κ is Boltzmann's constant (1.38×10^{-23} J/K), T is the gas temperature in Kelvin, and m is the molecular mass in kg. The vector $\bar{u}$ indicates the mean velocity whose magnitude is given in m/sec. Eq. 2 represents a Gaussian velocity distribution with a bandwidth (FWHM) of 0.265 a K Hz.

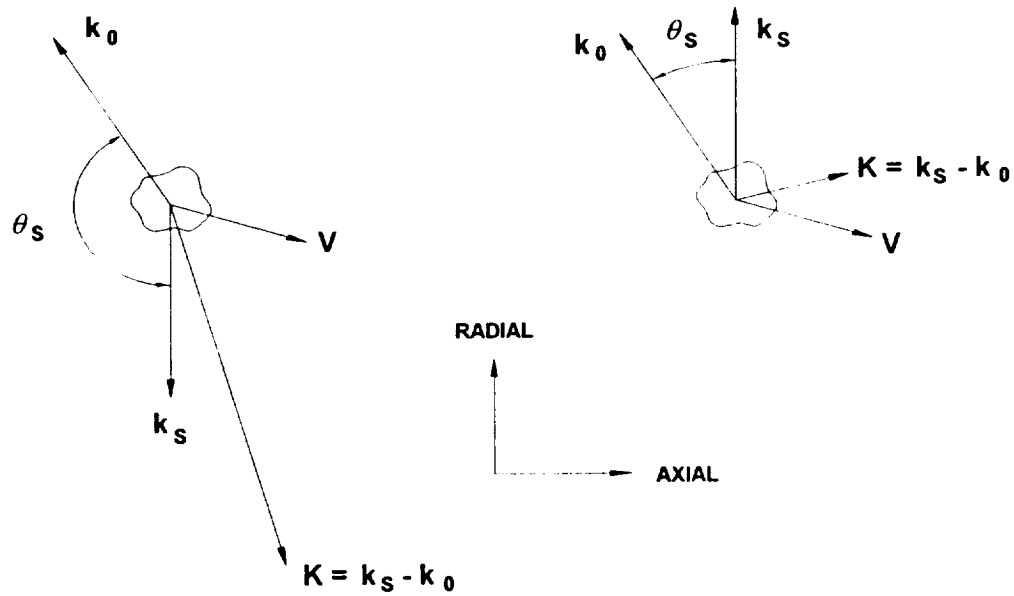

Fig. 2. Vector diagram of Rayleigh scattering: (a) backscatter and (b) forescatter.

For a single component gas with known molecular mass, the temperature can be extracted from the bandwidth of the observed scattered light. The mean velocity of the molecules can be found from the location of the peak of the Gaussian profile with respect to the incident wavelength as is shown in Fig. 3. The number density can be estimated from the total integrated Rayleigh scattered light. To obtain a density measurement, a reference measurement is necessary, where the total integrated Rayleigh scattering is measured with identical optical geometry on a gas with known number density and known differential scattering cross section. The number density measured is linearly proportional to the ratio of the total integrated Rayleigh scattering powers for both cases. The absolute number density can be found from the reference number density and ratio of differential scattering cross sections.

For a multi-component system with unknown composition, the total scattered Rayleigh profile can be assumed to be made up of the sum of the contributions from each individual species. If all species possess the same mean velocity, each contribution consist of a Gaussian lineshape located at the same spectral location with different spectral widths, dependent on the scatterers' molecular mass. The determination of temperature and number density from such a profile requires additional information. However, in many cases, a single species dominates the scattering process and a simple single component curve fit can yield the desired data.

4.2 Application.

Plumes of hydrogen-oxygen rockets consist predominantly of water vapor. Both pulsed and continuous wave (cw) strategies were employed to generate Rayleigh signals. The cw technique utilized the 514.5 nm line of a cw Argon-Ion laser. The pulsed strategy utilized the second harmonic output from an injection seeded Nd:Yag laser (λ = 532 nm, 150 MHz bandwidth). Both approaches satisfied the condition that the wavelength of the incident wave was much larger than the 1 nm effective diameter of the watermolecule. The light was vertically polarized and the detection direction, given in Eq.1 as the vector $\bar{k}_s$, was in a horizontal plane. This implies that the angle χ was 90°, which maximized the scattered power in the detection direction. The optical geometry for the cw strategy is shown in Fig. 4. Various steering optics

directed the laser beam through the optical port at 60°, parallel to the optical table mounted underneath the thruster, and between the diffuser and thruster. A 1000 mm focal length lens was used to focus the beam to a diameter of 180 μm in the near-field region of the thruster. Since stray laser light could impede the measurement by entering the detection system, extensive use was made of baffles, masks, high quality optical windows and beam stops. For the pulsed strategy, the laser beam was directed straight across the exit plane, with the detection from various angles.

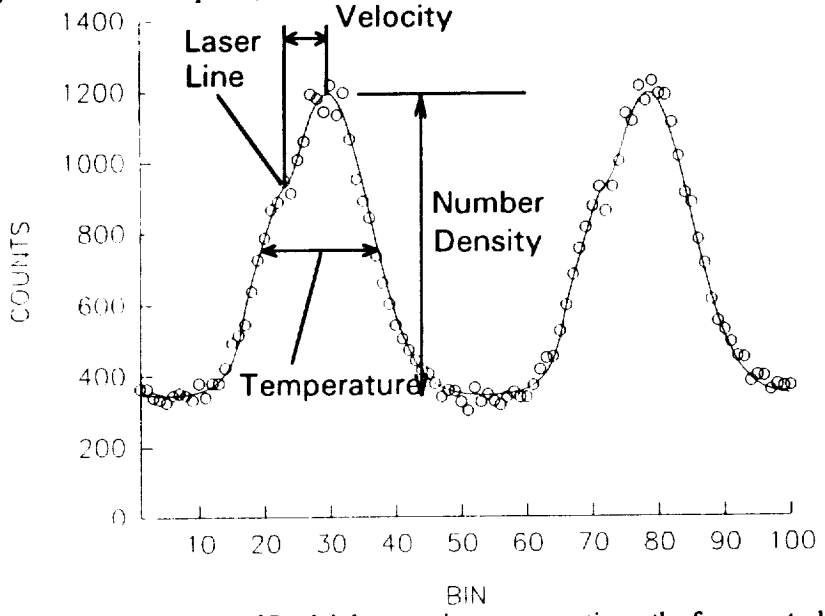

Fig. 3. Typical spectral scan of Rayleigh scattering over two times the free spectral range.

Two fiber optic collection probes were positioned at angles θ_s = 31° and 149° (see Fig. 2) for fore- and backscatter, respectively, to determine two components of the velocity. Each probe consisted of two lenses, one lens to collect scattered light and a second one to refocus it into a fiber, and a 10 m long fused silica fiber with a diameter of 1000 μm which gave an effective collection f# of 4.55. This geometry resulted in an adequate collection solid angle without introducing aperture broadening effects caused by the variation of collection angle over the collection optics. The fiber optic guided the scattered light through the altitude chamber bulkhead to an optical table, where the fiber output was collimated with an achromatic doublet and passed through a single pass scanning Fabry-Perot interferometer. The free spectral range of this interferometer was 21.4 GHz, sufficient to resolve the bandwidth (FWHM) of a nominal Doppler broadened Rayleigh spectrum of water (T≈1000 K, λ=514.5 nm, and θ_s=31°), which was approximately 6 GHz. The filtered light leaving the Fabry-Perot was focused through a 1000 μm aperture; collimated; passed through a multilayer dielectric interference filter to eliminate luminous background contributions; and detected with a 20% quantum efficiency, Gallium-Arsenide photomultiplier tube (PMT). A single threshold photon counter was used to measure the resulting Rayleigh scattering signal. Piezoelectric spacer elements were used to vary the Fabry-Perot mirror spacing over two adjacent orders of interference, thereby tuning the detected PMT signal through the Rayleigh spectrum. A typical spectral scan is displayed in Fig. 3.

Temperature and velocity were extracted from the measured Rayleigh spectrum by curve fitting a model function based on Eq. 1 to this spectrum. It was necessary to expand the model function to include the instrument response function. This instrument function was experimentally determined for both the unshifted, unbroadened argon-ion laser line, and the Nd:Yag second harmonic output. A small portion of laser light, reflected from the altitude chamber window was collected, attenuated with neutral density filters and coupled into a reference fiber. This fiber guided the light into the test section where it was mixed with the Rayleigh scattered light and collected with the collection probes. This reference signal could be turned on and off with the placement of a shutter on the collection side of the reference fiber. Excellent agreement was obtained between the experimentally measured and calculated reference spectra. For number density measurements, calibration spectra were obtained by traversing the measurement probe volume across the rocket exit plane while the facility was purged with a nitrogen gas of known temperature, density, and scattering cross section. High temperature spectra in the rocket plume were obtained at the same radial locations by traversing the probe volume along the path of the laser beam during a rocket fire.

Use of finite diameter optical fibers reduced the spectral resolution of the interferometer due to the increase in solid angle from the light collimated through the instrument.[7] This limited the sensitivity of the temperature measurement. Eq. 1 shows that the Doppler width was proportional to the magnitude of the scattering vector. This vector was much larger in the backscatter geometry, which caused the Doppler broadening to be much greater in the backscatter direction, surpassing the sensitivity of the instrument even at low temperatures (a theoretical limit of 245 K). As a result, temperature measurements could only be made in the backscatter geometry.

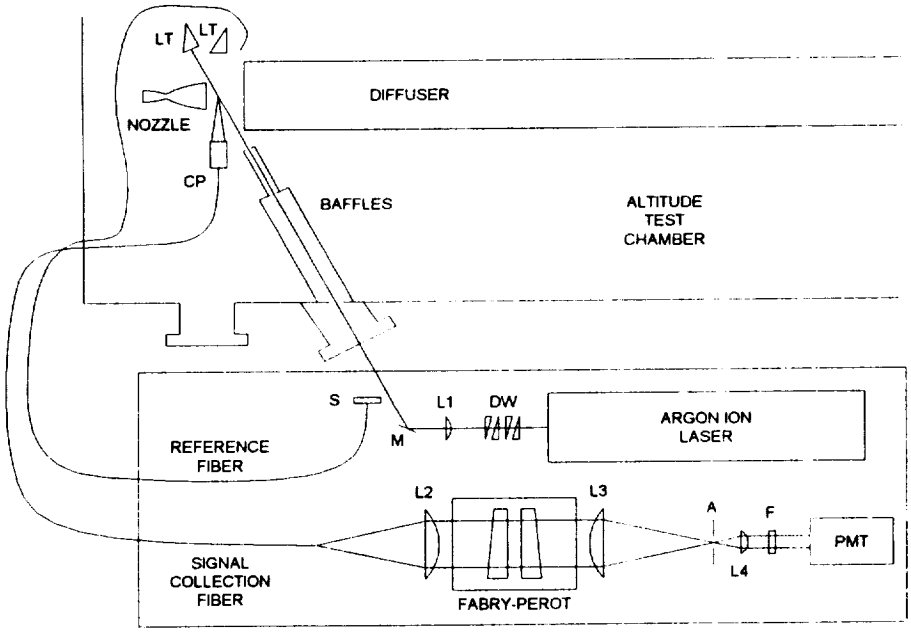

Fig. 4. Diagram of Rayleigh scattering optical arrangement with cw laser source.

An error analysis based on bias errors and the maximum likelihood parameter estimation procedure used in the curve fitting process, showed that the typical uncertainty in the mean velocity estimate was 200-300 m/s, independent of the magnitude of the mean velocity. Temperature determination was slightly less accurate, primarily due to the sensitivity of the estimation to noisy spectral profiles. Typical temperature uncertainty was 100-150 K. Number density estimates for a single component gas typically fall within 2-5% of the mean value.

5. VIBRATIONAL-ROTATIONAL RAMAN SCATTERING

Raman scattering is a process that occurs simultaneously with Rayleigh scattering when a plane electromagnetic wave is incident on a molecule with vibrational and rotational degrees of freedom. Because the internal molecular energy field changes during molecular vibration, the dipole induced by an incident wave changes accordingly. If the frequency of the incident wave is much higher than the molecular vibrational frequency, this change only becomes perceptible across many oscillations of the incident electric field. As a consequence, Rayleigh scattering which results from a constant oscillating dipole will be the dominant feature of the scattering spectrum. But a modulation of the dipole occurs with a period equal to the vibrational period of the molecule which results in the appearance of a much weaker spectral line shifted away from the Rayleigh frequency by a magnitude equal to the vibrational frequency. A similar spectral line appears due to the fluctuation in induced dipole during a molecular rotation. In this case, the period of change is half the period of one rotation since the molecular susceptibility towards dipole generation is equal for a molecule rotated 180°. The lines are therefore shifted away from the incident frequency by twice the rotational frequency.

A quantum mechanical description of this phenomenon is based on the exchange of energy between an incident photon and rotational-vibrational molecular energy modes. Since a molecule can only exist in discrete vibrational and rotational energy states, it absorbs enough of the energy of an incident photon to cause a transition to a upper energy state. The resulting "scattered" photon is less energetic and appears in the spectrum shifted to a lower frequency. Or in the case that

the molecule is already in an upper state, it might release enough energy to the photon to return to a lower energy state. It then scatters a more energetic photon which appears in the spectrum shifted to a higher frequency. Wave function calculations[8] show that vibrational transitions are only allowed between adjacent levels, which means a change of one vibrational quantum number. A vibrational transition to a upper energy level, given by a quantum change of $\Delta v = +1$, is referred to as Stokes scattering. A vibrational transition to a lower level, indicated by quantum change $\Delta v = -1$, is referred to as anti-Stokes scattering. Similar calculations show that rotational transitions are only allowed between every other level, thus corresponding to a rotational quantum number change of two. Scattering caused by rotational transitions given by quantum jump $\Delta J = +2$ are referred to as S-branch scattering. A change of $\Delta J = -2$ yields the O-branch and the pure vibrational transition $\Delta J = 0$ gives the Q-branch.

The energy of the scattered photon, and accordingly the spectral location at which it appears, depends on the amount of energy that has been exchanged with the molecule. This is equal to the difference between the two energy levels. Since these differences are unique for each molecule, the spectral line location can be used to identify the specific species that cause the scattering.

5.1 Theory

The distribution of the molecules over all possible energy levels of a gas volume in thermal equilibrium is described by the Boltzmann distribution. Since each of these molecules contributes to the scattered light, many lines appear in the spectrum that are shifted from the incident light. Vibrational and rotational motions of the molecules interact, with the magnitude of interaction dependent on the specific levels. Thus the amount of energy that is needed for a pure vibrational transition (Q-branch) of a single molecule, depends on the initial rotational level of that molecule. As a consequence, each rotational level in a pure vibrational transition appears at a different wavelength in the spectrum. The strength of each of these lines is directly proportional to the number of molecules in that specific rotational energy mode. The resulting distribution reflects the initial rotational distribution, which is an accurate indication of the rotational temperature. Because the differences in line locations are small, high resolution is needed to resolve the distribution. As the result of poor resolution and line broadening, they usually show up in the spectrum as one single line. Spectral lines caused by simultaneous rotational-vibrational transitions (O- and S-branches) lie further apart. However, these transitions have a lower transition probability, given by the Placzek-Teller coefficients. Accordingly, they are easier to resolve but more difficult to detect.

At higher temperatures, more vibrational levels become populated. As a result, upper vibrational transitions ($v=1\rightarrow2$, $v=2\rightarrow3$) cause new series of lines to appear, each representing the full rotational distribution of the particular vibrational state. The relative strength of each vibrational series reflects the molecular number density in that initial vibrational energy mode. Comparison of the different vibrational series line intensities gives the vibrational temperature. Comparing the total integrated scattering intensity over all transitions to that of a reference gas at known number density and temperature yields the species number density.

For a single component gas in thermal equilibrium, the total power scattered in the direction of observation in solid angle $d\Omega$ as the result of one allowable transition can be given as:[9]

$$P_{v',J'\rightarrow v'',J''}\, d\Omega = I_0\, n\, V_{sc} \left[\frac{d\sigma}{d\Omega}\right]_{\theta;\, v',J'\rightarrow v'',J''} S_{v',J'}\, d\Omega \qquad (3)$$

where I_0 is the incident irradiance in W/m^2, n the molecular number density in m^{-3}, and V_{sc} is the scattering volume in m^3. The differential Raman scattering cross section $\left[\frac{d\sigma}{d\Omega}\right]_{\theta;\, v',J'\rightarrow v'',J''}$ is given in m^2/sr. The shape function $S_{v',J'}$ reflects the Boltzmann distribution of the molecular population in its initial undisturbed state. This function only depends on the temperature, and is given by:

$$S_{v',J'} = \frac{g_n\,(2J'+1)}{Z}\, e^{-\left(\frac{E_{v',J'}}{\kappa T}\right)} \qquad (4)$$

where g_n is the nuclear spin factor. This factor is a weighting factor which reflects the naturally occurring difference in spin populations between the even and odd rotational distributions (ortho- and para- states) of diatomic homonuclear molecules and is 1 for heteronuclear molecules. For example, for hydrogen, the even:odd ratio is 1:3, for nitrogen, this ratio is 2:1, and for oxygen, the even states are missing and its nuclear spin factor $g_n = 0$ for the even lines, which means that transitions starting from even rotational energy levels do not exist. The partition function Z is the rotational-vibrational probability distribution of the molecules over all possible energy states and the energy $E_{v',J'}$ is the rotational-vibrational energy of the initial molecular state. A single prime, ', refers to the initial molecular state and the double prime, ", to the final state.

The differential Raman scattering cross section depends on the type of scattering molecule, the specific rotational-vibrational transition, and the fourth power of the frequency of the scattered wave. It also depends on the angle θ between the incident and the scattered radiation, on the polarization of the incident and observed radiation, and on the angle between the incident electric field vector and the direction of observation. For any specific experiment, the last three species independent properties remain constant. The dependence of the scattering cross section for a particular species is on the wavelength of scattering and the specific transition. Measured values of the scattering cross sections for different species are usually given for a specific optical configuration and incident wavelength. They are tabulated as the ratio between this cross section and the scattering cross section of the nitrogen Q-branch,[10] for which the absolute values are well documented. Corrections for different experimental optical characteristics and wavelength can be implemented accordingly.[11,12]

It is often not necessary to know the absolute scattering cross section as long as the different dependencies are accounted for. The type of species can be determined from the spectral location where scattered light is observed, and the temperature can be determined from the intensity distribution of the scattered spectrum. The underlying profile of this distribution reflects the Boltzmann population and as such is a direct thermometer. To extract an accurate value for the temperature, the shape of the basic distribution has to be corrected for its dependence on the rotational-vibrational quantum numbers. The change in scattering cross section as a function of transition type and scattering wavelength has to be accounted for. The functional dependence is:

$$\left[\frac{d\sigma}{d\Omega}\right]_{\theta,\, v',J' \rightarrow v'',J''} \propto P_{J,\Delta J}\,(v'+1)\,(\nu_0 - \nu_{RS})^4 \qquad (5)$$

where $P_{J,\Delta J}$ are the rotational quantum number dependent Placzek-Teller coefficients.[13] A different J-dependent coefficient exists for each of the rotational branches (O-,Q- and S-branch). The term $(v'+1)$ indicates the vibrational dependence of the line strength of the Stokes transition. This term becomes (v') for the anti-Stokes transition, indicating that from the vibrational ground state $(v' = 0)$ such a transition does not exist. The term ν_0 is the frequency of the incident wave and ν_{RS} is the Raman shift. This shift is the energy difference between the initial and final energy state of the transition divided by Planck's constant, and is species dependent.

After the temperature has been extracted, the species number density can be determined. The ratio of the total scattered power versus the total scattered power of the nitrogen Q-branch obtained under known conditions gives the number density. To obtain high accuracy, the number density and temperature of a reference sample of the measured species must be carefully controlled. This sample can then be used as a secondary calibration standard.

5.2 Application

A full description of the Raman diagnostics facility is given in Ref. 14. The layout of the facility is displayed in Fig. 5. A flashlamp pumped dye laser, lasing at a nominal wavelength of 595 nm, was directed across the plume to generate spontaneous Raman scattering. The pulse length was approximately 2 μsec and the nominal pulse energy about 1 Joule/pulse. The bandwidth (FWHM) of the incident radiation was 0.03 nm (or 0.9 cm^{-1}). A pulsed input was chosen to minimize the background luminosity by gating the detection equipment. Use of a shorter pulse length and/or shorter wavelength incident radiation created concern about laser induced gas breakdown.[15] For wavelengths in the ultraviolet region, fluorescence signals exceeded the Raman scattering signals. Furthermore, at longer wavelengths, individual Raman transition lines are further apart, allowing a better resolution of the band profile. An additional advantage of a wavelength in the visible is that conventional optical components could be used for transmission and manipulation. However, because the scattered intensity scales with the fourth power of the scattering wavelength the signal levels are smaller at longer wavelength ranges. The decay in laser pulse energy as a function of time was continuously monitored by splitting 1% of the pulse energy off and directing it to a pulse energy meter.

The pulsed beam was coupled into an 800 μm optical fiber of 20 m length which guided it through the high altitude facility bulkhead. The pulse emanating from the fiber was collimated and refocused in the exit plane of the rocket nozzle. The optical axis lay in a plane perpendicular to the thruster axis. Receiving optics with an f# of 2.4 were mounted in the same plane perpendicular to the incident optics. These optics consisted of a collection lens and a refocusing lens which coupled the detected scattering into a 20 m length, 800 μm diameter optical fiber. This fiber guided the scattered light through the altitude chamber bulkhead into a diagnostics room. The scattered light emanating from this fiber was collimated and filtered with a Raman notch filter with a better than 10^6 signal attenuation at the laser line. The light was focused into a 0.5 m spectrometer with 300 or 1200 groove grating, dependent on the application. For simultaneous multispecies detection, the 300 groove grating gave a 6.4 nm/mm spectral resolution. This allowed simultaneous detection of oxygen, hydrogen, nitrogen and water with a single 25 mm array detector. For temperature measurements where line shapes were important, a 1200 groove grating with a 1.6 nm/mm resolution was used.

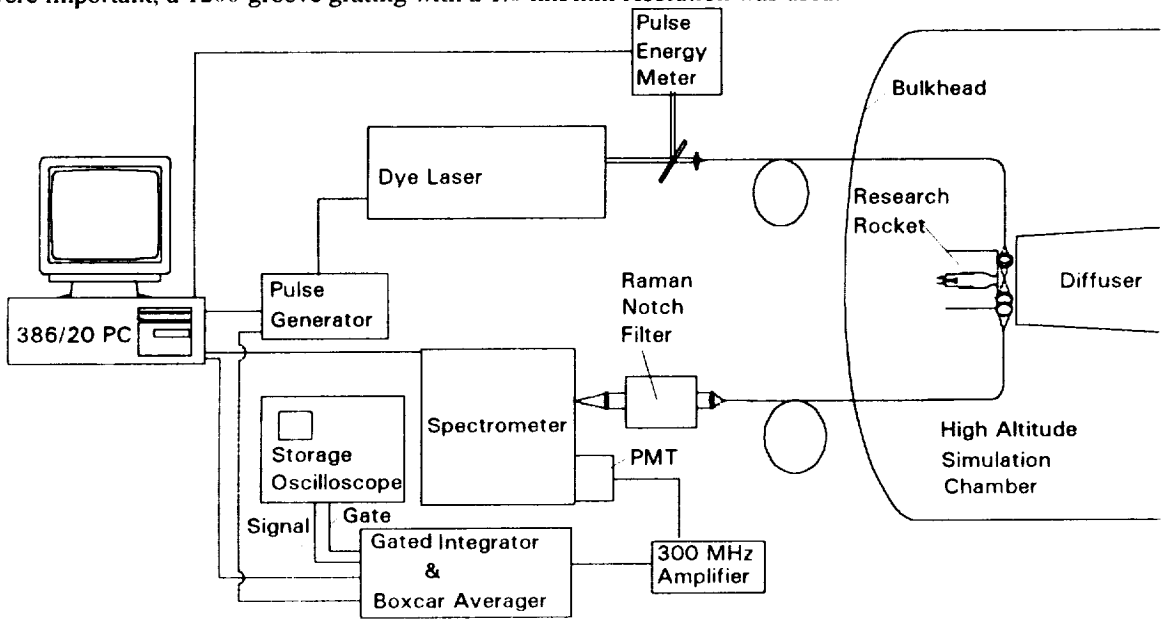

Fig. 5. Schematic of Raman diagnostics data acquisition system.

Two detection schemes were used. A 700 pixel linear array with 25μm pixel size was gated such that the gate was coincident with the laser pulse. With the use of background subtraction, this pulsed system could extract very weak signals from the noise. The measured temperature could be extracted from the measured line shapes using a model function based on Raman theory and the instrument function of the detection equipment. Calibration factors were obtained from a reference gas at known temperature and number density. A maximum likelihood parameter estimation procedure completed the data reduction. The instrument function was measured using a helium neon laser line and a mercury lamp. Oxygen and

nitrogen spectra obtained in atmospheric air were used as calibration spectra. Typical nitrogen spectra, both measured and calculated, for two different temperatures are shown in Fig. 6. The spectrometer entrance slit width for these measurements was 200 μm.

At very low number densities and limited test time, the linear array did not provide sufficient sensitivity. Therefore a GaAs photomultiplier tube with a higher quantum efficiency (Q.E.=12% @ 700 nm) was used. A boxcar averager and integrator was used to gate and integrate the PM tube signal with optimum noise rejection as is shown in Fig. 5. With an exit slit of 200 μm a nominal spectral resolution of 0.33 nm was obtained. By scanning the spectral range of interest and integrating at each spectral location over 300 laser pulses, a spectral profile could be obtained. For very weak signals it was necessary to open the spectrometer entrance slit further to allow more light. The 800 μm collection fiber had a Numerical Aperture (N.A.) of 0.22. Collimating and refocusing optics projected a 800 μm image of the collection fiber exit on the spectrometer entrance slit, slightly over filling the (110x110 mm) grating. For maximum light transmission, the entrance and exit slit were set to 800 μm. The resolution of this method however was significantly worse than the linear array and the test time needed for a full spectrum was quite long. The linear array method was therefore preferable in cases that the signal intensity was sufficient.

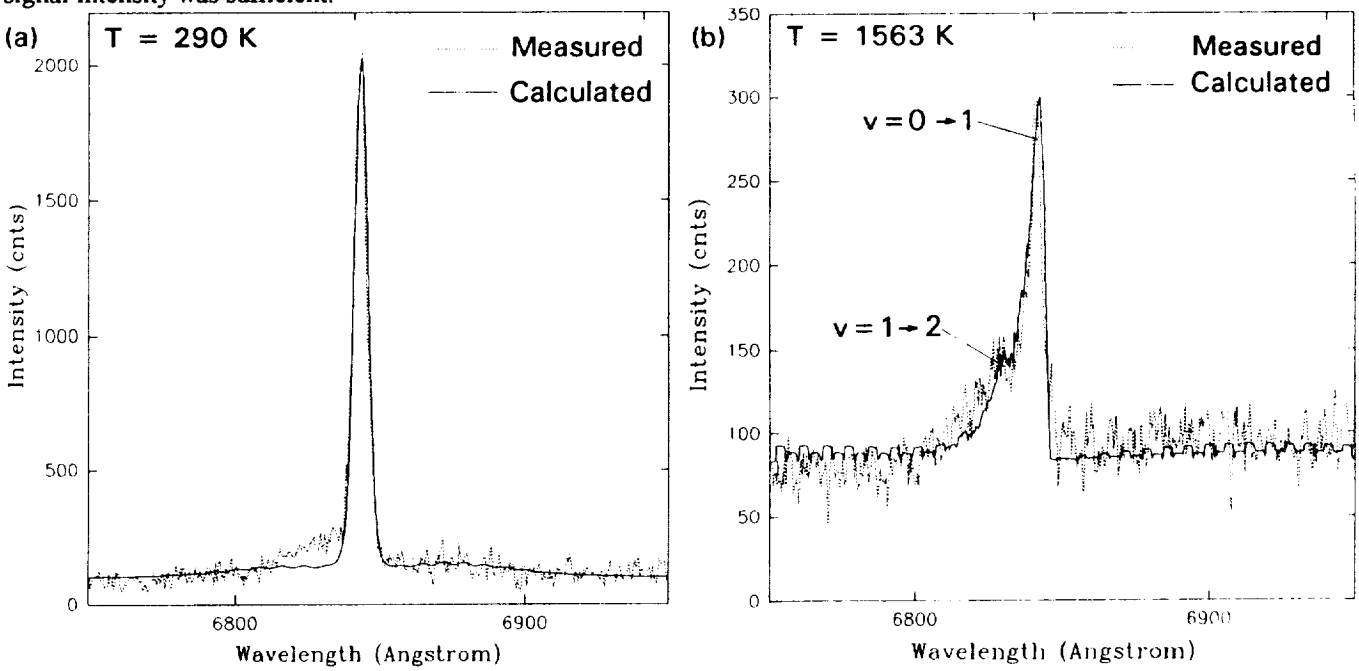

Fig. 6. Measured and calculated Raman Q-branch spectra of nitrogen at two different temperatures: (a) T=290 K; (b) T=1563 K.

6 RESULTS

6.1 Rayleigh scattering results

Temperature, velocity, and species number density measurements made with the cw Argon-Ion laser on a different rocket engine were reported in an earlier paper.[4,7] Preliminary results of pulsed velocity measurements on the above described engine are shown in Fig. 7. Axial and radial velocities were compared against flow field predictions obtained using the RPLUS-code.[16] Temperature and number density estimates were not reliable due to uncertainty in the species composition in the exit plane of this rocket. The presence of oxygen in the core caused a distortion of the pure Gaussian shape based on scattering water molecules that was the basis of the model function. Vertical error bars included both the random statistical error associated with photon noise as well as bias errors caused by uncertainty in the scattering angles and Fabry-Perot mirror spacing. The horizontal error bars represent the spatial sampling extent of the probe volume which was approximately 3 mm in radial direction. The actual uncertainty in the center position of the probe volume was on the order of 0.5 mm.

The RPLUS code has the capability of making near-field plume predictions for expansion in a vacuum, yet can not accomodate flow expansion into a finite pressure environment. Experimental conditions imposed a finite back pressure on the exhaust flow. Since Rayleigh measurements were done parallel to the exit plane at 3 mm downstream, some discrepancies were expected at the perimeter of the exhaust jet, but the core was expected to be unaffected. The axial velocity profile showed a considerable discrepancy between the measured and predicted values, both at the perimeter and at the core. It was believed that the difference in velocity gradient was caused by a stronger mixing between the fuel-film cooling and oxygen rich core flow than was modeled. This enhanced mixing would lead to a gradually varying molecular weight with radius and accordingly would cause a gradually varying velocity going radially outwards. The measured axial velocity in the core was lower than the predicted velocity. These differences were attributed to differences in the species composition and energy release in the core.

The radial velocity profile showed qualitative agreement with the predicted values, especially close to the core. Further from the core in radial direction the discrepancy increases. It was expected, however, that the back pressure caused the expansion to be confined, whereas the predicted expansion was free, allowing uninhibited expansion to occur. This effect was most significant at the outermost point. In general, the radial velocity was well predicted, indicating that the nozzle divergence was adequately modeled. This conclusion was also supported by previous measurements obtained using cw Rayleigh scattering in the plume of a different nozzle,[7] where similar good agreement in radial measurements was obtained.

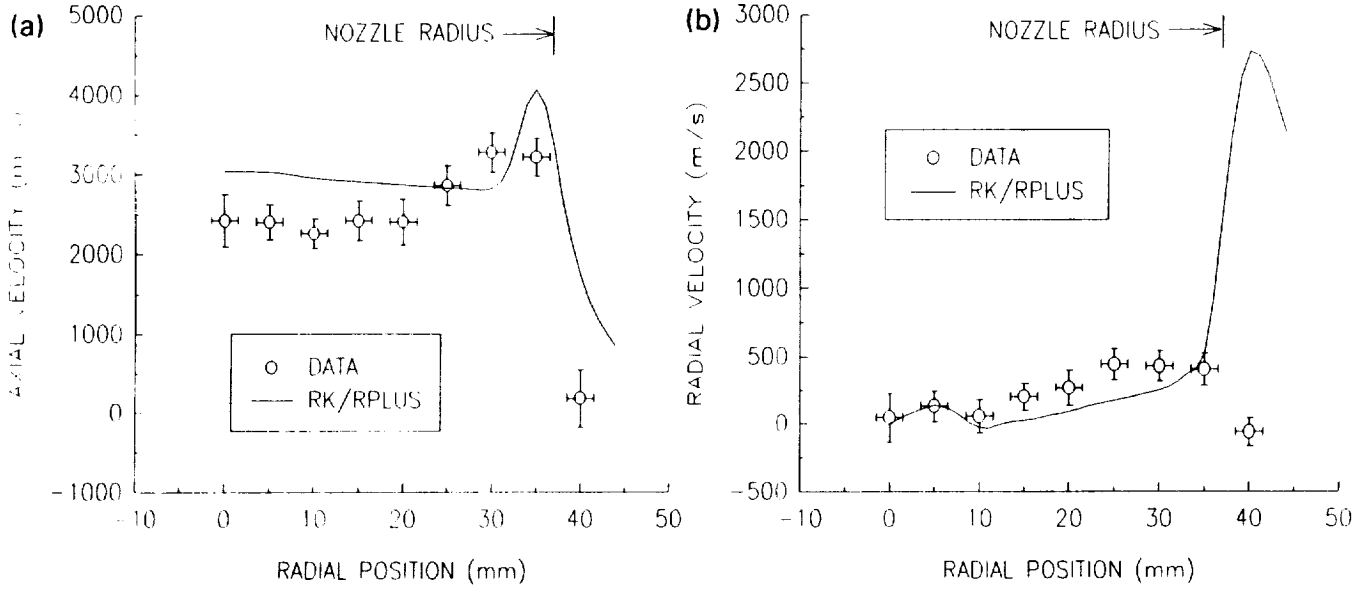

Fig. 7. Comparison of Rayleigh velocity data with numerical RPLUS-code prediction: (a) axial velocity component, (b) radial velocity component.

6.2 Spontaneous Raman Scattering Results

Spontaneous Raman scattering was used to measure species densities and temperatures. However number densities predicted in the exit plane of a full nozzle were on the order of 10^{16} cm^{-3}, and tests showed that Raman scattering was too weak to obtain reliable results over the limited test periods. The nozzle was therefore shortened to a 1.86:1 ratio, and Raman measurements were completed in a plane 10 mm downstream of this exit plane. Since the nozzle was severely underexpanded, it was expected that the back pressure would not have a significant effect. Even at this location, a relatively low number density was expected, and a PMT with scanned spectrometer was used. Of all the major species expected (hydrogen, oxygen, and water), only oxygen and water vapor generated a detectable Raman signal. The oxygen signal was strong enough to allow extraction of accurate data. The water vapor spectrum, due to its spread as the result of high temperature and its many Raman lines, could not be clearly defined over the limited (30 sec.) test time. Temperature and oxygen number densities were extracted from the Stokes line, with calibration factors obtained from oxygen in air.

Measured temperature and oxygen number density profiles are shown in Fig. 8a and b, respectively, at 10 mm downstream of the shortened nozzle, along with profiles predicted by the RPLUS code. Species detection at this location have implications for the the general quality of combustion chamber mixing and combustion efficiency. Both predicted and measured temperature profiles showed qualitative agreement, but the magnitude of the measured temperature was about 10% higher and increased towards the perimeter of the plume. The local maximum in the predicted density profile at about 5 mm radial position, was caused by a weak compression wave. Such a wave would not be detectable with the Raman scattering diagnostics. The corresponding local maximum in the measured temperature profile was thought to be caused by the shear layer mixing and combustion between the fuel-film and the oxygen rich core. This caused a higher temperature away from the core. This was also predicted in the model, as was shown in the temperature profile at the exit plane (dashed line), where the effects of the compression wave and shear layer coincided at about 7 mm radial location. However, in the prediction where expansion in vacuum was assumed, this high temperature peak propagated away from the core and was at about 12.5 mm radial location when it reached the plane where measurements were taken. As previously mentioned, the presence of the back pressure and the diffuser during the measurements limited the expansion. Vibrational non-equilibrium of the exhaust gases at the measurement location could be the cause of the difference between the measured and predicted temperatures. The temperature was not measured beyond 7.5 mm radially because no oxygen was detected at those locations.

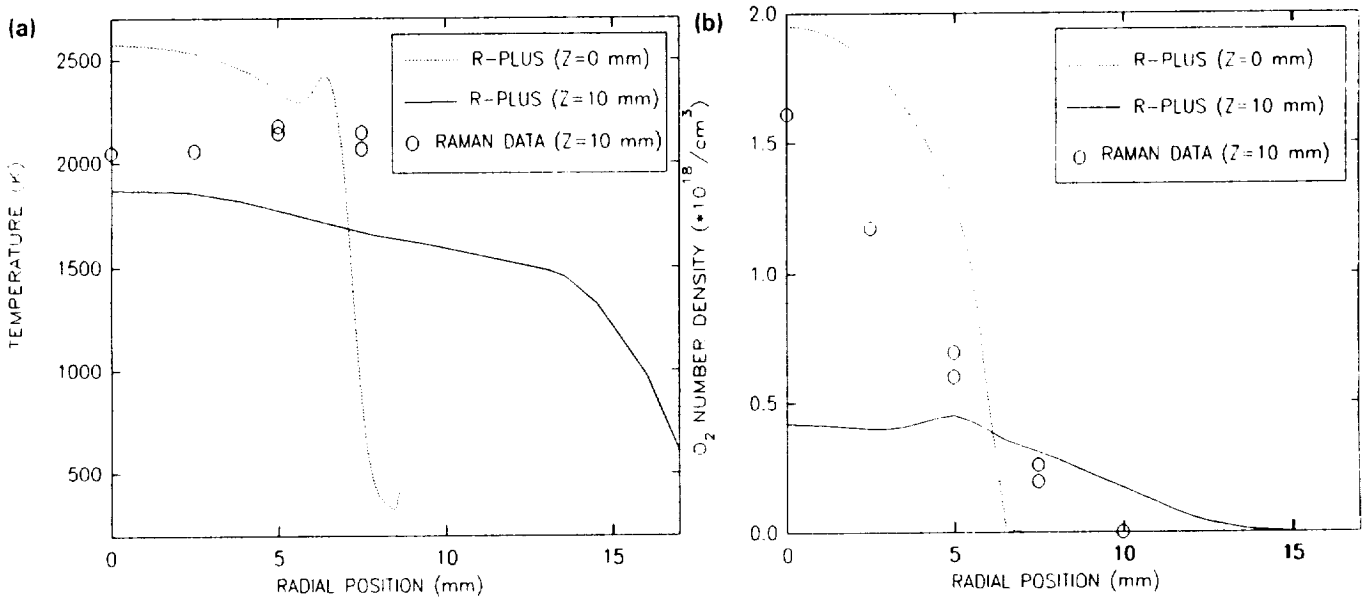

Fig. 8. Raman data in the exit plane of a low area ratio nozzle: (a) temperature, (b) O2 number density.

The measured oxygen number density profile was significantly different than the predicted profile in both magnitude and shape. Again, the solid line represents predictions at the 10 mm downstream plane where measurements were taken and the dashed line represents exit plane conditions. Both the measured radial gradient and number density magnitude lie in between the two predicted locations. It is believed that the difference was caused by inadequacies in injector modeling. The model assumed plug flow for injection, with homogeneous concentrations and temperature throughout, and with constant velocity. Mixing between this core flow and the fuel film takes place in the shear layer originating behind the bluff fuel-film insert. It was concluded from the measurements, however, that the injector flow was stratified, with combustion at the perimeter, where good mixing between oxygen and hydrogen occurred. Measurements also suggest that hydrogen did not penetrate the core flow, leaving the final injection flow very much stratified in number density, and to a lesser degree in temperature and velocity. Mixing took place between the oxygen rich injector flow and fuel film, but was not sufficient to fully mix over the short distance to the throat. The core remained oxygen rich. This was reflected by the measured profile, where the number density of oxygen in the core at 10 mm downstream was almost identical to the predicted number density at the exit plane. The same reason caused the measured radial profile to be much steeper, further magnified by the fact that the experimental radial expansion was slower than the predicted expansion in vacuum, as was mentioned earlier.

A check of the experiment with mass conservation was not possible since water number densities could not be measured, even though water did show up as a very weak spectrum. In agreement with predictions, hydrogen could not be detected due to the low number densities. Because of its low molecular weight and the fast expansion at the perimeter of the plume in vacuum, number densities at the measurement location were calculated to be of the order of 1016 cm-3. This was below the detectable limit.

7 CONCLUDING REMARKS

Rayleigh and Raman scattering have successfully been applied to determine velocity, temperature and species number densities in the plume of a low thrust hydrogen-oxygen rocket installed in a high altitude chamber. Both cw and pulsed Rayleigh data and pulsed Raman data were obtained. Much of the transmission of incident and collected radiation was facilitated by the use of optical fibers, which were an integral part of the diagnostics equipment. They permitted a reduction of stray and scattered light by reducing the number of optical windows. These fibers also provided flexibility in design and installation. Optimizing the fibers for diameter and radiation wavelength provided a powerful and multifaceted diagnostics facility.

The measured radial velocity profile was closely predicted by a viscous nozzle code, RPLUS. The measured axial profile significantly differed from predictions, both in magnitude and distribution. The cause of this discrepancy was attributed to inadequate modeling of the turbulent shear layer mixing in the combustion chamber. Temperature and number densities were extracted from the Rayleigh measurements based on assumptions about the species composition. Raman scattering data showed that the oxygen number density was different from values predicted using the CFD code. Because oxygen has a strong influence on the shape of the Doppler signal, these Rayleigh temperature and number density results for the rocket under investigation were not reliable.

The measured temperature profile determined from Raman scattering spectra was approximately 10% higher than predicted. This may be the result of vibrational non-equilibrium. Also the expansion was modeled to occur in a vacuum. The experimental expansion was much more confined, giving a higher temperature than predicted. Discrepancies also exist between the measured and predicted oxygen number density. This was attributed to the initial conditions in the code, which included a homogeneous plug flow entering the combustion chamber. In addition, difficulties in accurately modeling the turbulence in the shear layer between the fuel-film and the core region was thought to contribute to the differences .

Hydrogen spectra could not be detected and water spectra were too weak to yield accurate results. Raman scattering therefore is a more powerful diagnostic technique in a high number density environment, such as in the combustion chamber. Vibrational-translational relaxation problems in a supersonic flow biased the temperature measurement toward the vibrational temperature. However, with better detection equipment and a longer available test time, vibrational non-equilibrium effects in the nozzle flow could be studied.

8. ACKNOWLEDGMENTS

The authors wish to thank Dr. Richard Seasholtz for his assistance and useful discussions concerning the implementation of the Rayleigh scattering diagnostic and the analysis of the spectral profiles. They also wish to thank Roger Scheman for his invaluable assistance during this project.

9.REFERENCES

1. D. C. Byers, "Advanced Onboard Propulsion Benefits and Status," *NASA TM-103174*, March 1989.

2. P. J. Robinson, "Space Station Auxiliary Thrust Chamber Technology," *NASA CR-185296 Final Report 2210-90-FR*, July 1990.

3. G. P. Richter and H. G. Price, "Proven, Long-Life Hydrogen/Oxygen Thrust Chambers for Space Station Propulsion," *NASA TM-88822*, JANNAF Propulsion Meeting, New Orleans, Aug. 1986.

4. R. G. Seasholtz, F. J. Zupanc, and S. J. Schneider, "Spectrally Resolved Rayleigh Scattering Diagnostic for Hydrogen-Oxygen Rocket Plume Studies," *J. of Propulsion and Power*, Vol. 8, pp. 935-943, Sept.-Oct. 1992.

5. R. P. Sandoval and R. L. Armstrong, "Rayleigh-Brillouin Spectra in Molecular Nitrogen," *Phys. Rev.*, Vol. A13, pp. 752-757, 1976.

6. L. A. Arrington and S. J. Schneider, "Low Thrust Rocket Test Facility," *AIAA 26th Joint Propulsion Conference Paper AIAA-90-2503*, June 1990.

7. F. J. Zupanc and J. M. Weiss, "Rocket Plume Flowfield Characterization Using Laser Rayleigh Scattering," *AIAA 28th Joint Propulsion Conference Paper AIAA-92-3351*, July 1992.

8. G. Placzek, "Rayleigh-Streuung und Raman-Effect," Handbuch der Radiologie, Vol. VI, E. Marx, Ed., Akademische Verlagsgesellschaft, Leipzig, 1934.

9. J. A. Wehrmeyer, T-S. Cheng and R. W. Pitz, "Raman scattering measurements in flames using a tunable KrF excimer laser," *Applied Optics*, Vol. 31, No. 10, pp. 1495-1504, 1992.

10. H. W. Schroetter and H. W. Kloeckner, "Raman Scattering Cross Sections in Gases and Liquids," Topics in Current Physics: Raman Spectroscopy of Gases and Liquids, A. Weber, Ed., pp. 123-166, Springer Verlag, Berlin, 1979.

11. T. Hirschfeld, "Correction of Raman Cross Section from Laboratory to Remote Spectrometer Geometries," *Applied Spectroscopy*, Vol. 27, No. 5, 1973.

12. A. C. Eckbreth, Laser Diagnostics for Combustion Temperature and Species, Ch. 5, Abacus Press, Cambridge MA, 1988.

13. G. Herzberg, Molecular Spectra and Molecular Structure I: Spectra of Diatomic Molecules, pp. 127-128, 2nd Ed. Reprint, Krieger Pub. Co., Malabar FL, 1989.

14. W. A. de Groot, "The Development of a Fiber Optic Raman Temperature Measurement System for Rocket Flows," *AIAA 27th Joint Propulsion Conference Paper AIAA-91-2316*, June 1991.

15. D. C. Smith and R. G. Meyerand, "Laser Radiation Induced Gas Breakdown," Principles of Laser Plasmas, G. Bekefi, Ed., pp. 457-508, Wiley Interscience, New York, 1976.

16. J. M. Weiss and C. L. Merkle, "Numerical Investigation of Reacting Flow fields in Low -Thrust Rocket Engine Combustors," *AIAA 27th Joint Propulsion Conference Paper AIAA-91-2080*, June, 1991.

REPORT DOCUMENTATION PAGE

Form Approved
OMB No. 0704 0188

Public reporting burden for this collection of information is estimated to average 1 hour per response, including the time for reviewing instructions, searching existing data sources, gathering and maintaining the data needed, and completing and reviewing the collection of information. Send comments regarding this burden estimate or any other aspect of this collection of information, including suggestions for reducing this burden, to Washington Headquarters Services, Directorate for information Operations and Reports, 1215 Jefferson Davis Highway, Suite 1204, Arlington, VA 22202-4302, and to the Office of Management and Budget, Paperwork Reduction Project (0704-0188), Washington, DC 20503.

1. AGENCY USE ONLY (*Leave blank*)	2. REPORT DATE	3. REPORT TYPE AND DATES COVERED
	January 1993	Technical Memorandum

4. TITLE AND SUBTITLE

Laser Rayleigh and Raman Diagnostics For Small Hydrogen/Oxygen Rockets

5. FUNDING NUMBERS

WU-506-42-31

6. AUTHOR(S)

Wilhelmus A. de Groot and Frank J. Zupanc

7. PERFORMING ORGANIZATION NAME(S) AND ADDRESS(ES)

National Aeronautics and Space Administration
Lewis Research Center
Cleveland, Ohio 44135-3191

8. PERFORMING ORGANIZATION REPORT NUMBER

E-7540

9. SPONSORING/MONITORING AGENCY NAMES(S) AND ADDRESS(ES)

National Aeronautics and Space Administration
Washington, D.C. 20546-0001

10. SPONSORING/MONITORING AGENCY REPORT NUMBER

NASA TM-105999

11. SUPPLEMENTARY NOTES

Prepared for the SPIE International Symposium on Lasers, Sensors, and Applications sponsored by the Society of Photo-Optical Instrumentation Engineers, Los Angeles, January 16–23, 1993.

12a. DISTRIBUTION/AVAILABILITY STATEMENT

Unclassified - Unlimited
Subject Category 20 and 72

12b. DISTRIBUTION CODE

13. ABSTRACT (*Maximum 200 words*)

Localized velocity, temperature, and species concentration measurements in rocket flow fields are needed to evaluate predictive computational fluid dynamics (CFD) codes and identify causes of poor rocket performance. Velocity, temperature, and total number density information have been successfully extracted from spectrally resolved Rayleigh scattering in the plume of small hydrogen/oxygen rockets. Light from a narrow band laser is scattered from the moving molecules with a Doppler shifted frequency. Two components of the velocity can be extracted by observing the scattered light from two directions. Thermal broadening of the scattered light provides a measure of the temperature, while the integrated scattering intensity is proportional to the number density. Spontaneous Raman scattering has been used to measure temperature and species concentration in similar plumes. Light from a dye laser is scattered by molecules in the rocket plume. Raman spectra scattered from major species are resolved by observing the inelastically scattered light with a linear array mounted to a spectrometer. Temperature and oxygen concentrations have been extracted by fitting a model function to the measured Raman spectrum. Results of measurements on small rockets mounted inside a high altitude chamber using both diagnostic techniques are reported.

14. SUBJECT TERMS	15. NUMBER OF PAGES
Rayleigh scattering; Raman scattering; Hydrogen/Oxygen rockets	16
	16. PRICE CODE: A03

17. SECURITY CLASSIFICATION OF REPORT	18. SECURITY CLASSIFICATION OF THIS PAGE	19. SECURITY CLASSIFICATION OF ABSTRACT	20. LIMITATION OF ABSTRACT
Unclassified	Unclassified	Unclassified	

National Aeronautics and
Space Administration

Lewis Research Center
Cleveland, Ohio 44135
SPDT-1

Official Business
Penalty for Private Use $300

FOURTH CLASS MAIL

ADDRESS CORRECTION REQUESTED

U.S.MAIL

Postage and Fees Paid
National Aeronautics and
Space Administration
NASA 451

NASA